Slow-electron collisions with CO molecules in an exact-exchange plus parameter-free polarization model

Ashok Jain
Department of Physics, Florida A&M University, Tallahassee, Florida 32307

D. W. Norcross
Joint Institute for Laboratory Astrophysics, University of Colorado and National Institute of Standards and Technology, Boulder, Colorado 80309-0440

(Received 28 June 1991)

We report low-energy (0.001–10-eV) electron-CO scattering cross sections obtained using an exact-exchange (via a separable-exchange formulation) plus a parameter-free correlation-polarization model in the fixed-nuclei approximation (FNA). The differential, total, and momentum-transfer cross sections are reported for rotationally elastic, inelastic, and summed processes. To remove the limitations of the FNA with respect to the convergence of total and differential cross sections, the multipole-extracted-adiabatic-nuclei approximation is used. The position and width of the well-known $^2\Pi$ shape-resonance structure in the cross section around 2 eV are reproduced quite well; however, some discrepancy between theory and experiment in the magnitude of the total cross section in the resonance region exists. We also present results for $^2\Pi$ shape-resonance parameters as a function of internuclear separation. Differential-cross-section results agree well with the measurements of Tanaka, Srivastava, and Chutjian [J. Chem. Phys. **69**, 5329 (1978)] but are about a factor of 2 larger than the results obtained by Jung *et al.* [J. Phys. B **15**, 3535 (1982)] in the vicinity of the $^2\Pi$ resonance.

PACS number(s): 34.80.Bm, 34.80.Gs

I. INTRODUCTION

In this paper, we are concerned with vibrationally and electronically elastic scattering of slow (0.001–10 eV) electrons by the CO molecule. The role of CO in several applied sciences such as lasers, gas discharges, plasmas [1], and MHD power generation [2] has made it both interesting and important to investigate its interaction with low-energy electrons. In the past, the *e*-CO system has been studied extensively both in the laboratory [3–21] (including swarm [17–20] and electron transmission [21] experiments) and by theorists [22–36]. This list of earlier studies is not complete and does not include other processes such as vibrational and electronic excitation, dissociation, etc.

It is now feasible to carry out *ab initio* calculations on electron-molecule collisions at the exact-static-exchange (ESE) and ESE plus polarization (ESEP) levels under the fixed-nuclei approximation (FNA) or taking into account the nuclear vibration explicitly in the total Hamiltonian of the electron-molecule complex. Most applications of these sophisticated numerical techniques have, however, been mainly limited to homonuclear targets (see Collins and Schneider [37] for a recent review). It is still very difficult to carry out a full ro-vibrational close-coupling calculation for any molecular target, even for the simplest molecule H_2, although some progress is being made [38].

A major problem in the FNA is that for polar molecules the forward differential and total cross sections do not converge due to the neglect of the rotational Hamiltonian in the scattering formulation [39,40]. Nevertheless, the momentum-transfer cross section is still well defined [29]. There have been several theoretical studies of the *e*-CO system at the ESE level [33,34,36] (polarization effects neglected) and using a static- (model) exchange (SME) plus polarization (SMEP) approach [25–32]. The *R*-matrix calculation of Salvini *et al.* [36], the first ESEP calculation, was devoted to a study of the $^2\Pi$ resonance and the momentum-transfer cross section. To the best of our knowledge, the present work is the first and only calculation of CO differential and total cross sections in which exchange is treated exactly and a parameter-free polarization potential used. The most important differences between our approach and that of Salvini *et al.* [36] are that the *R*-matrix method approaches the treatment of correlation via a one-hole two-particle scheme, whereas we use an approach based on electron-gas theory. We include the effect of long- (terms that go as $1/r^4$) as well as short-range polarization of the target molecule by the projectile electron. It will thus be very interesting to compare the results of the present ESEP calculation with the results of Salvini *et al.*

Here we report the details of our *ab initio* calculations on the *e*-CO system; a preliminary report has appeared elsewhere [41]. The target molecule is treated at the near-Hartree-Fock level. The electron exchange problem is solved exactly via the separable form of the exchange kernel [42], and polarization effects are included via a parameter-free correlation-polarization (CP) potential [43] that is a simple function of the target charge density and known molecular polarizabilities. The scattering cal-

culations are carried out in the molecular body-fixed frame; i.e., molecular rotation is neglected in this step. It is subsequently included using a variant of the FNA that also corrects for the complete breakdown of the conventional adiabatic approximation for polar molecules noted above.

We present differential (DCS), integral (σ_t), and momentum-transfer (σ_m) cross sections for rotationally elastic, inelastic, and summed (including thermal averaging over the Boltzmann distribution of rotational states) processes. We also present results for the $^2\Pi$ shape resonance [width $\Gamma(R)$ and position $E_r(R)$] as a function of internuclear separation R, which are found to be in very good agreement with recent measured values. Some discrepancies between theory and measurement with respect to the magnitude of the total and differential cross sections in the resonance region, the DCS for forward scattering, and the momentum-transfer cross section at low energies, are pointed out and discussed.

In the following section we provide a summary of our method and numerical procedures. In Sec. III, the results are presented and discussed, while Sec. IV contains concluding remarks. We use atomic units throughout until otherwise specified.

II. THEORETICAL MODEL AND THE NUMERICAL PROCEDURE

Most of the details of the present approach have been discussed earlier [44–46]; here we provide a brief account only. We employ a standard technique in the single-center integral-equation formalism of the close-coupling theory under the FNA. This technique, originally developed to deal with local model-exchange and polarization potentials [47], has been modified [48] to treat electron exchange exactly via the separable expansion technique [42]. The resulting coupled integral equations are solved in the molecular body-fixed (BF) frame of reference for each symmetry (Λ) separately at a given geometry of the molecule. Thus, we neglect the nuclear motion term in the total Hamiltonian of the e-CO collision system.

All our calculations are performed using a near-Hartree-Fock wave function for the CO target. We generate a Gaussian-type-orbital (GTO) basis set for the ground configuration of the CO molecule ($1\sigma^2 2\sigma^2 3\sigma^2 4\sigma^2 5\sigma^2 1\pi^4; X\,^1\Sigma^+$) by using a standard molecular structure code [49]. The same functions are used with a set of generalized-valence-bond computer codes [50] to calculate the separable form of the exchange kernel,

$$K(\mathbf{r},\mathbf{r}')=\sum_{\alpha}\chi_\alpha(\mathbf{r})\gamma_\alpha\chi_\alpha(\mathbf{r}')\ , \tag{1}$$

where the orthonormal GTO functions $\chi_\alpha(\mathbf{r})$ give a diagonal representation of the exchange kernel with eigenvalues γ_α. We include several diffuse functions on both centers and also at the center of mass (c.m.) of the molecule (to represent bonding functions). Since the same basis set is used for both target and separable exchange expansion, it is necessarily different for each scattering symmetry. Thus the basis set at all centers (C/c.m./O) is taken to be

Σ: $(10s6p2d/3s3p/6s6p2d)$ $[6s4p2d/3s3p/6s4p2d]$,

Π: $(10s6p2d/3s3p2p/10s6p2d)$ $[6s4p2d/3s3p2p/6s4p2d]$,

Δ: $(10s6p2d3d/3s3d/10s6p2d3d)$ $[6s4p2d3d/3s3d/6s4p2d3d]$.

Here we have used a standard convention to denote the primitives (( )) and contracted ([ ]) GTO's. The two extra p functions at the c.m. in the $^2\Pi$ symmetry have exponents of 0.003 and 0.001. In the Δ state, the diffuse functions are the three d functions on the carbon atom with exponents 0.2, 0.08, and 0.04; three d functions on the oxygen atom with exponents 0.55, 0.10, and 0.08, and three d functions on the c.m. with exponents 0.007, 0.003, and 0.001. Note that we removed all $3p$ functions from the c.m. in the Δ symmetry. For Φ symmetry we used a conventional free-electron gas model for the exchange potential [39]. For higher symmetries, exchange was neglected and a unitarized version of the first-ordered Born approximation (FBA) was used for all the scattering calculations [44].

The above GTO basis gave molecular properties as listed in Table I and compared with other selected data (theoretical and experimental). There are a large number of theoretical studies on the structural properties (energy, moments, polarizabilities, etc.) of CO at the multiconfiguration self-consistent-field (MCSCF) level. It is not possible to include all of them in Table I; we have, however, listed those values that we have used in the present calculation and the Hartree-Fock-limit results for the multipole moments of the CO molecule [52,54]. We see from Table I that there is large difference between the theoretical and experimental values of the dipole moment of CO at R_{eq}; in order to partly compensate for this error, we have used the experimental values of the dipole and quadrupole moments when producing the final cross sections via the multipole-extracted-adiabatic-nuclei (MEAN) approximation (see below).

In brief, we solve the following set of coupled integral equations (after carrying out all the single-center expansions of the potential and scattering function) for the radial components of the continuum function belonging to a particular symmetry Λ (symbol Λ suppressed in the following equation),

TABLE I. Molecular data (in a.u.) for the CO molecule at R_{eq}.

Parameter	Present data	Other calculations	Experiment
Energy	−112.7708	−112.7891 [52]	−113.377 [55]
Dipole moment (D)	0.0993	0.105 [52]	−0.0441 [56]
Quadrupole moment (Q)	1.5424	1.634 [52]	1.44 [57]
Octupole moment (Ω)	4.58	4.407 [54]	
Polarizabilities			
α_0		13.13 [51]	13.34 [53]
α_2		2.61 [51]	2.39 [53]
R_e			2.132 [58]
Rotational constant ($\mathcal{B}$) (cm^{-1})		1.9313 [58]	

$$\left[\frac{d^2}{dr^2}-\frac{l(l+1)}{r^2}+k^2\right]f_{ll_0}(r) = \sum_{l'}\left[V_{ll'}(r)f_{l'l_0}(r) + \sum_{\alpha}\chi_\alpha^l(r)\gamma_\alpha\int_0^\infty \chi_\alpha^{l'}(r')f_{l'l_0}(r')dr'\right], \quad (2)$$

where the potential matrix $V_{ll'}$ includes static as well as polarization terms. In Eq. (2), $\chi_\alpha^l(r)$ and γ_α arise from the separable form of the exchange kernel (1), and $\chi_\alpha^l(r)$ is the radial part obtained by projecting GTO's onto a spherical harmonic, i.e.,

$$\chi_\alpha^l(r)=r\int d\hat{\mathbf{r}}\chi_\alpha(\mathbf{r})Y_l^m(\hat{\mathbf{r}}) . \quad (3)$$

The method of solving the scattering Eq. (2) is given in Ref. [42]. The static potential is included exactly at the Hartree-Fock level by using the GTO basis as described above.

The polarization effects are included free of adjustable parameters via the correlation-polarization (CP) model [43]. In the CP potential approach the correct asymptotic forms $-(1/2r^4)\alpha_0$ and $-1/2r^4\alpha_2P_2(\cos\theta)$ are joined to the corresponding moments of a free-electron-gas model of the correlation potential at their crossing points. The polarizabilities at R_{eq}, α_0 (13.34 a.u.), and α_2 (2.39 a.u.), are taken to be the experimental values [53]. The values of $\alpha_0(R)$ and $\alpha_2(R)$ at seven other R values are taken from the calculations of Greedy, Bacskay, and Hush [54]. (In Refs. [59–62] more *ab initio* calculations are presented for the multipole moments, polarizabilities, etc., as a function of R.) In Fig. 1 we show the spherical part of the potential matrix V_{00} for both the static and polarization terms for the equilibrium internuclear separation. It is interesting to note that the correlation energy at the crossing point is about 0.9 eV, the same as found for other closed-shell molecular targets [43].

In order to include the contribution of the long-range dipole field in all the close-coupling K-matrix elements, we integrated Eq. (2) up to a radius $r_{max}\sim 10l/k$; thus at very low energies the value of r_{max} reaches a few thousand atomic units. We made several other convergence tests on the K-matrix elements (including the eigenphase sums and the partial total cross sections) keeping the convergence criterion to better than 1%. This included the number of terms ($\bar{\lambda}_{max}$) in the single-center expansion of the static potential, the size of the close-coupling K-matrix (l_c), and the expansion size of the exchange kernel (1) in terms of α_{max} and $l(l_x)$. These values along with few other quantities (see below) are given in Table II.

As mentioned earlier, in the FNA the DCS and σ_t do not converge for polar molecules. In order to produce meaningful values of both cross sections, we use the

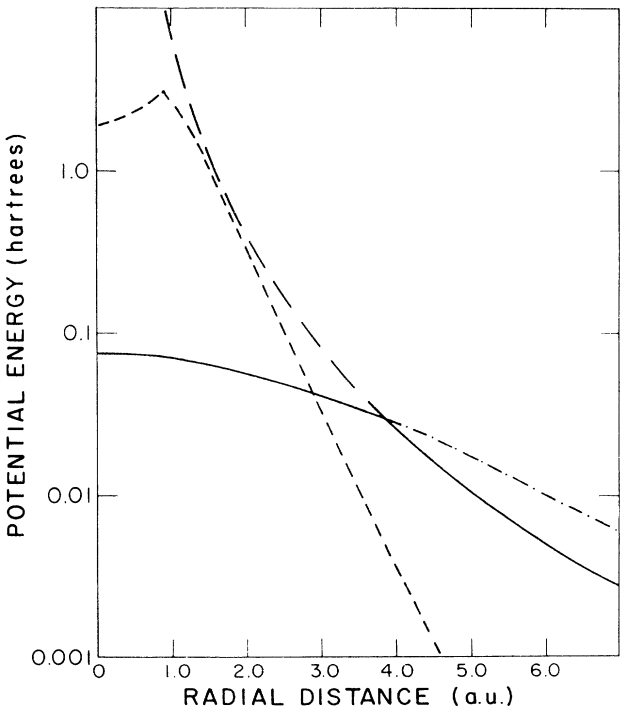

FIG. 1. Spherical part of the e-CO potential at equilibrium: — — —, static; —·—·—·, correlation potential beyond the crossing point; — — , $-\alpha_0/2r^4$ potential inside the crossing point; ——, correlation-polarization (CP) potential.

TABLE II. Convergence parameters for *e*-CO scattering calculations. For explanation of notation, see the text.

Parameter	Value
$\bar{\lambda}_{max}$	40 (only 20 for the electronic term)
l_c	19 (implies 20 channels)
α_{max}	25 (Σ), 17 (Π), 13 (Δ)
l_x	16 (Σ), 21 (Π), 16 (Δ)
l_t	5
λ_{max}	24 ($l_t=0,1,2,3$); 19 ($l_t>3$)
l_b	48
l_{max}	72 for $l_t=1$ and 2; 48 otherwise

MEAN approximation [63], which is a generalization of the completeness formula given by Crawford and Dalgarno [24]. In the MEAN approximation the DCS for a particular $J\rightarrow J'$ rotational excitation in the laboratory or space-fixed (SF) frame is expressed as

$$\frac{d\sigma}{d\Omega}(J,J')=\frac{d\sigma^{\mathrm{FBA}}}{d\Omega}(J,J') + \frac{k_{J'}}{4k_J}\sum_{l_t}[C(Jl_tJ';00)]^2\frac{1}{k^2} \times\sum_{\lambda=0}^{\lambda_{max}}(B_{\lambda,l_t}-B^{\mathrm{FBA}}_{\lambda,l_t})P_\lambda(\cos\theta) , \tag{4}$$

where the first term in Eq. (4) is the usual closed-form expression for rotational excitation in the FBA in the SF frame, k_J and $k_{J'}$ are, respectively, the initial and final wave vectors, $C(\ )$ is a Clebsch-Gordan coefficient, and l_t is the angular momentum transferred during the collision. The B_{λ,l_t} are the expansion coefficients of the DCS obtained from the close-coupling scattering equations, while the $B^{\mathrm{FBA}}_{\lambda,l_t}$ are the corresponding quantities in the FBA, evaluated in the BF coordinate system under the FNA scheme. The initial and final wave vectors are related by

$$k_J^2-k_{J'}^2=\mathcal{B}[J'(J'+1)-J(J+1)] , \tag{5}$$

where $\mathcal{B}$, the rotational constant of CO, is given in Table I.

In Eq. (4), the second term vanishes for high values of λ_{max} due to cancellation effects. This is important for the dipole case ($l_t=1$) for which $B_{\lambda,1}$ and $B^{\mathrm{FBA}}_{\lambda,1}$ individually diverge. Equation (4) achieves similar corrections for the quadrupole (moment and the polarizability) terms. In our calculations, the B_λ coefficients were evaluated for a few BF electron energies (k^2) in the range 0.0005–10 eV; the final results at any desired SF energy, defined by Eq. (5) and the geometric mean $k^2=k_Jk_{J'}$, are obtained by the interpolation of these coefficients on a natural cubic spline.

We summarize the size of various expansion parameters in Eq. (4) used to implement the MEAN methodology in the following. The evaluation of the B_{λ,l_t} coefficients is done in terms of the l_t-reduced T matrices, namely

$$T^{l_t}_{ll'}=\sum_\Lambda(-1)^\Lambda C(ll'l_t;\Lambda-\Lambda)T^\Lambda_{ll'} , \tag{6}$$

where Λ represents the index for a particular symmetry ($\Lambda=0$ for Σ, $\Lambda=1$ for Π, $\Lambda=2$ for Δ, $\Lambda=3$ for Φ, and so on). We included T matrices for $\Lambda\leq 3$ only from the solution of Eq. (2), while for $\Lambda>3$ we used the unitarized Born approximation [44] (UBA). For $\Lambda=3$ the close-coupling T matrices agree with the UBA values to within 1%. These were augmented by the UBA T matrices for $l_c<l\leq l_b$, and for $l_t=1$ and 2 by the FBA T matrices for $l_b<l\leq l_{max}$.

The values of l_b and l_{max} were determined from the λ sum in Eq. (4). For the purpose of our convergence criterion (1%), we need a large value of λ (say λ_{max}) such that the second term in Eq. (4), i.e., $B_{\lambda,l_t}-B^{\mathrm{FBA}}_{\lambda,l_t}$, vanishes for $\lambda\geq\lambda_{max}$. For $l_t=0$, λ_{max} was chosen large enough (see Table II) that the B_λ coefficients behaved as $\sim 1/\lambda$; the sum from $\lambda_{max}+1$ to ∞ was evaluated in closed form. These values are shown in Table II. It is to be noted that the evaluation of σ_t requires only the $\lambda=0$ component, while for σ_m we need only $\lambda=0$ and 1. As a general rule, good convergence requires $l_b\geq 2\lambda_{max}$; our value $l_b=48$ is sufficient for all l_t. For $l_t=1$ and 2, the contributions to the sum in Eq. (4) cancel identically for $l>l_b+\lambda_{max}$; this determines l_{max} (see Table II). As mentioned earlier, we used experimental values of the dipole and quadrupole moment and quadrupole polarizability in order to remove partially the deficiencies of the Hartree-Fock approximation. This is essential in the case of CO, where the difference between experimental and Hartree-Fock-level dipole moments is quite large (Table I).

The expressions for the total ($\sigma_t^{JJ'}$) and the momentum-transfer ($\sigma_m^{JJ'}$) cross sections are evaluated from Eq. (4) for any (JJ') rotational transition. The total (summed over all final rotor states) integrated (σ_t) and momentum-transfer (σ_m) cross sections are easily obtained from

$$\sigma_t(J)=\sum_{J'}\sigma_t^{JJ'},\quad \sigma_m(J)=\sum_{J'}\sigma_m^{JJ'} . \tag{7}$$

For comparison with some measurements the energy loss or stopping cross section is also of interest. This is defined by

$$\sigma_s(J)=\sum_{J'}(k_J^2-k_{J'}^2)\sigma_t^{JJ'} . \tag{8}$$

We recall that in the limit $k_{J'}/k_J\simeq 1$, i.e., the incident electron energy k^2 is much larger than the spacing between rotational states undergoing transitions, Eqs. (4), (7), and (8) simplify considerably, since the second term in Eq. (4), when summed over J', becomes independent of J. The results are [63]

$$\frac{d\sigma}{d\Omega}(J)=\sum_{J'}\frac{d\sigma^{\mathrm{FBA}}}{d\Omega}(J,J') + \frac{1}{4k^2}\sum_{l_t}\sum_{\lambda=0}^{\lambda_{\max}}(B_{\lambda,l_t}-B_{\lambda,l_t}^{\mathrm{FBA}})P_\lambda(\cos\theta)\ , \tag{9}$$

$$\sigma_t(J)=\sum_{J'}\sigma_t^{\mathrm{FBA}}(J,J')+\frac{\pi}{k^2}\sum_{l_t}(B_{0,l_t}-B_{0,l_t}^{\mathrm{FBA}})\ , \tag{10}$$

$$\sigma_m(J)=\sum_{J'}\sigma_m^{\mathrm{FBA}}(J,J') + \frac{\pi}{k^2}\sum_{l_t}[(B_{0,l_t}-B_{0,l_t}^{\mathrm{FBA}}) -\tfrac{1}{3}(B_{1,l_t}-B_{1,l_t}^{\mathrm{FBA}})]\ , \tag{11}$$

and

$$\sigma_s(J)=\sum_{J'}\sigma_s^{\mathrm{FBA}}(J,J') + \frac{\pi}{k^2}\sum_{l_t}\mathcal{B}l_t(l_t+1)(B_{0,l_t}-B_{0,l_t}^{\mathrm{FBA}})\ . \tag{12}$$

For a proper comparison with some experiments, we also average σ_t, σ_m, and σ_s over a Boltzmann distribution of initial rotational states at temperature T. These averaged values are denoted by $\langle\sigma_t\rangle_T$ and $\langle\sigma_m\rangle_T$ or $\langle T\rangle$. This is a relatively simple exercise, since the dependence on J and J' in Eq. (4) is confined to the first FBA term, and to the kinematic and algebraic factors in the second term. In the limit that $k_{J'}/k_J\simeq 1$, the Boltzmann averaging process clearly involves only the first terms in Eqs. (9)–(12), since the second terms in these expressions are all independent of J.

The MEAN approximation cannot be used uncritically near rotational thresholds, but, to the extent that the second term in Eq. (4) yields only a small correction to the SF-frame FBA, it may be useful even in this energy range. For energies or processes for which $d\sigma/d\Omega(J,J')$ (when summed over J'), $\sigma_t(J)$, $\sigma_m(J)$, or $\sigma_s(J)$ prove to be insensitive to J, we can also be relatively confident that the MEAN approximation is valid. All of the results to be presented later in this paper can be reproduced with a few simple FBA formulas and a relatively compact set of tables of the coefficients B_{λ,l_t} and $B_{\lambda,l_t}^{\mathrm{FBA}}$. These are available on request.

III. RESULTS AND DISCUSSION

A. Parameters of the $^2\Pi$ shape resonance

Low-energy e-CO scattering is dominated by the well-known $^2\Pi$ shape resonance around 2 eV, which has a width of about 1 eV [64,65]. The occurrence of such resonances in electron-molecule scattering, including CO, is discussed in a review by Schulz [66]. The measured σ_t cross sections [10–14] clearly reveal this feature, as do the swarm [17–20] and transmission [21] experiments. The success of any theoretical model depends very much upon the accuracy of its $^2\Pi$ resonance parameters as compared to observed values. In the past, most calculations have been limited to some kind of fitting procedure, e.g., using pseudopotentials in a semiempirical approach [25–32]. The only parameter-free results available for the e-CO $^2\Pi$ resonance parameters at the *ab initio* ESEP level are from the R-matrix calculation of Salvini, Burke, and Noble [36]. At the ESE level, Levin, Flifet, and McKoy [33] and Collins, Robb, and Morrison [34] have also reported results on the $^2\Sigma$ and $^2\Pi$ states of the CO molecule.

The parameters of the $^2\Pi$ shape resonance [values of $\Gamma(R)$ and $E_r(R)$] can be derived from the eigenphase sums (δ_s) by fitting to the Breit-Wigner formula [67]. Figure 2 illustrates the $^2\Pi$ δ_s at the equilibrium geometry (R_{eq}) obtained in the present work in various models. The $^2\Pi$ resonance is clearly very sensitive to the treatment of exchange and polarization effects. It is worth mentioning here that in a phenomenological approach it

TABLE III. $^2\Pi$ shape-resonance parameters (position E_r and width Γ in eV) for e-CO collisions from various calculations and measurements. Calculated and measured resonance parameters are not strictly equivalent, as the former are determined by fitting eigenphase sums to the Breit-Wigner profile while the latter are obtained by analysis of the integrated cross section, respectively.

	ESE		ESEP	
	E_r	Γ	E_r	Γ
Present results	3.30	1.91	1.85	0.95
Levin, Fliflet, and McKoy [33]	3.4±0.1	1.65±0.15		
Collins, Robb, and Morrison [34]	3.54	2.07		
Salvini, Burke, and Noble [36]	3.02	1.61	1.72	0.75
Collins and Schneider[a]	3.31	1.84		
Collins and Schneider[a]	3.25	1.80		
Ehrhardt *et al.* [7] (expt.)			2.0	0.4
Szmythkowski and Zubek [10] (expt.)			1.5	0.75
Kwan *et al.* [12] (expt.)			1.9	
Buckman and Lohmann [14] (expt.)			1.95	
Tronc, Azria, and LeCoat [65] (expt.)			1.8	1.0

[a]As given in Ref. [36].

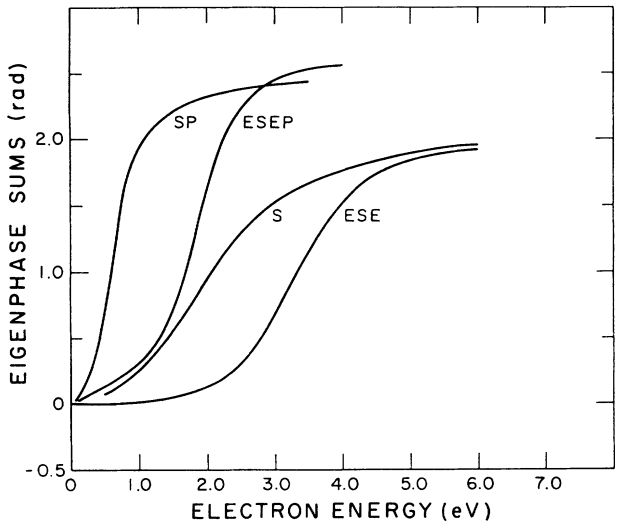

FIG. 2. *e*-CO $^2\Pi$ resonance eigenphase sums in various models: *S*, pure static; ESE, exact-static-exchange; SP, *S* plus polarization; and ESEP, ESE plus polarization.

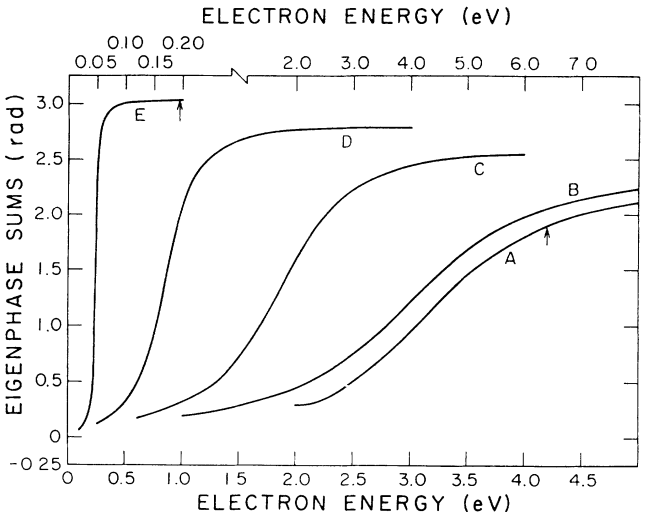

FIG. 3. Eigenphase sums for the $^2\Pi$ symmetry at various internuclear geometries: *A*, $R = 1.7318$; *B*, 1.9318; *C*, 2.1318; *D*, 2.3318; and *E*, 2.5318. An arrow indicates the upper energy scale to be followed. Curves without an arrow follow the bottom energy scale.

is very difficult to get correct behavior with respect to both the position and the width of a resonance feature; e.g., if the value of the resonance position (E_r) is fitted, the width may come out to be quite different than observed (see Ref. [30]).

We present our $E_r(R_{eq})$ and $\Gamma(R_{eq})$ values from the analysis of δ_s in the ESE and ESEP models along with various other theoretical and experimental data in Table III. It is very encouraging to get such remarkably good agreement between the present parameter-free ESEP model and several measurements [12,14,65]. Our ESE values for the position and width of the shape resonance agree best with the calculations of Collins and Schneider, cited in Ref. [36]; both of their calculations used the linear algebraic approach, but differed in the numerical treatment of exchange. Differences with the ESE results of Salvini, Burke, and Noble [36] are most probably due to the use of different target wave functions. Our ESEP results are in somewhat better agreement with those from the *R*-matrix calculation [36] than are the two corresponding ESE results. In addition to the use of different target wave functions, long-range polarization was neglected in the *R*-matrix calculation, and short-range correlation effects were included in their ESEP calculations using virtual molecular orbitals. This could have partially compensated for differences in the target wave functions. As mentioned earlier, there is no semiempirical procedure involved in either set of ESEP calculations. In this energy region, long-range polarization effects do not appear to be of critical importance.

In Fig. 3, the present ESEP results for δ_s are shown as a function of energy for a range of *R* values. At large separation, the resonance becomes very sharp and shifted to quite low energy. The corresponding values of $E_r(R)$ and $\Gamma(R)$ are depicted in Fig. 4 along with the *R*-matrix results of Salvini, Burke, and Noble [36]. There is gen-

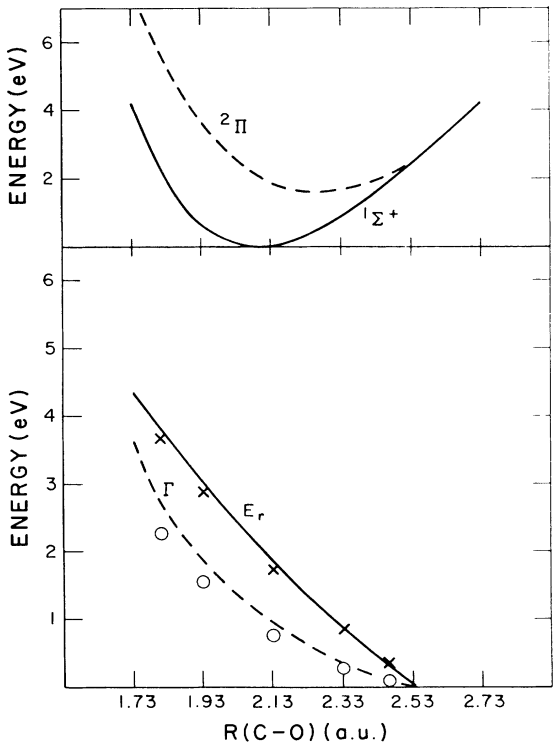

FIG. 4. Upper set of curves: $^1\Sigma^+$ and $^2\Pi$ states of CO and CO^-, respectively. Bottom set: width [$\Gamma(R)$] and position [$E_r(R)$] relative to neutral curve of the $^2\Pi$ resonance as a function of *R*. The crosses and open circles are the calculations of Salvini, Burke, and Noble (Ref. [36]) for E_r and Γ, respectively.

eral agreement between the present and the R-matrix calculations. Also shown in this figure are the potential energy curves for the CO $^1\Sigma^+$ state (the present Hartree-Fock GTO basis set) and for the CO^- $^2\Pi$ state. From the present data on $E_r(R)$ and $\Gamma(R)$ for the CO^- ion, cross sections for the dissociative channels can be determined [68].

B. Cross sections

We now present our ESEP results for cross sections. Figure 5 displays the partial integrated cross sections for the $^2\Pi$, $^2\Sigma$, and $^2\Delta$ symmetries over the whole energy range considered here. (These were obtained directly from the calculations in the molecular body-fixed frame, and are thus, strictly speaking, unconverged for a polar molecule. The point here is to illustrate the relative contributions from various scattering symmetries.) The $^2\Pi$ symmetry clearly shows the shape-resonance feature, while a minima is occurring in both the $^2\Sigma$ and $^2\Pi$ symmetries at very low energies (below 0.5 eV). The contribution from the $^2\Delta$ symmetry is small at all energies considered here and so is that from higher-order symmetries (not shown).

1. Differential cross sections

In Fig. 6 we show the overall behavior of the DCS as function of energy at several angles between 5° and 150°. The DCS curves clearly depict the $^2\Pi$ shape resonance around 2 eV, but the effect of the shape resonance is prominent only for scattering angles below 90°. The p and d waves in $^2\Pi$ scattering are mainly responsible for this resonance behavior.

The total DCS's at 1.8, 2.1, 3.0, 5.0, 7.5, and 10 eV are presented in Figs. 7 and 8 along with the measured values of Tanaka, Srivastava, and Chutjian [9] and Jung *et al.* [15]. Our DCS values are generally higher than the measured values of Tanaka, Srivastava, and Chutjian [9] for smaller angles. The discrepancy is quite similar to that noted when comparing [45] our earlier work on HCN with measurements by the same group. Integrated cross sections obtained from these measurements will be compared with our results below. The values of Jung *et al.* at 1.8 and 2.1 eV have been multiplied by a factor of 2 to emphasize the excellent qualitative agreement between theory and experiment. In this energy range our integrated cross section (see below) is also larger than several measured values, but only by about 30%. For impact energies $\gtrsim 1.5$ eV, the DCS is dominated by elastic transitions ($l_t=0$) for angles $\lesssim 45°$, whereas $l_t=1$ and 2 transitions contribute significantly for intermediate angles. Transitions for which $l_t=2$ make the largest single contribution at intermediate angles for energies $\gtrsim 5.0$ eV.

Sohn *et al.* [16] have reported absolute measurements

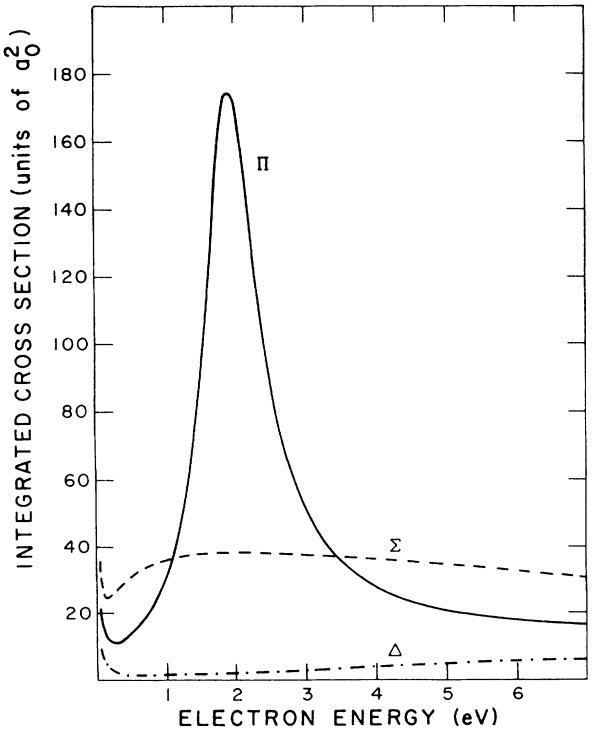

FIG. 5. Partial BF-frame integrated cross sections for e-CO scattering for $^2\Sigma$, $^2\Pi$, and $^2\Delta$ symmetries in the present ESEP model as a function of energy.

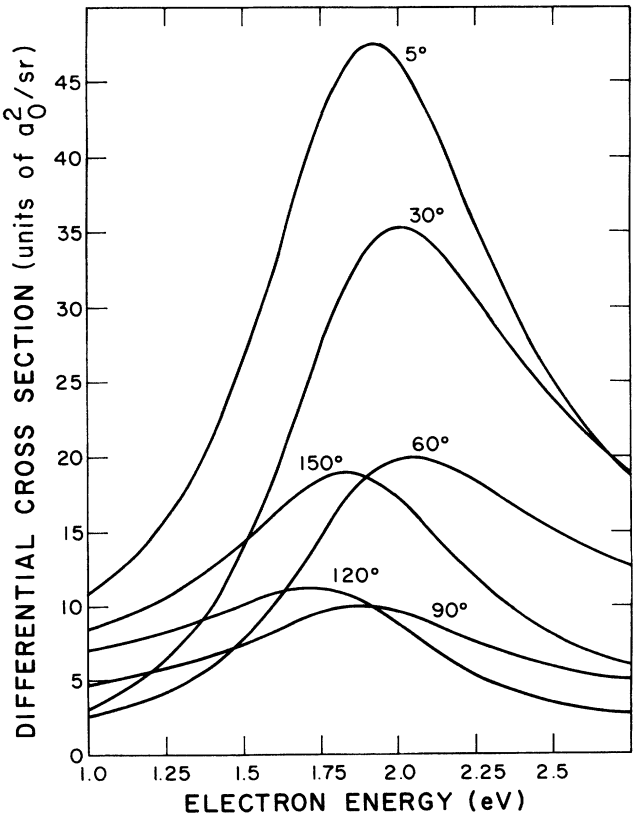

FIG. 6. Rotationally summed differential cross sections for e-CO scattering as a function of energy at several scattering angles. At these energies the DCS is independent of the initial rotor state.

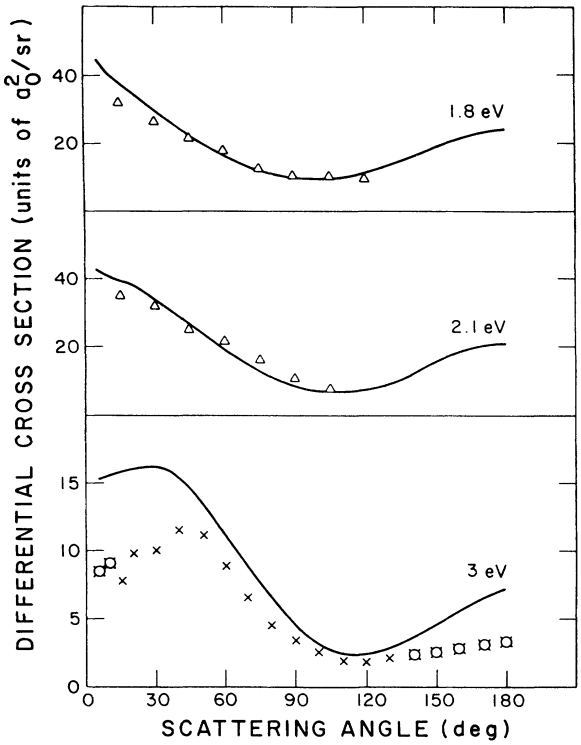

FIG. 7. Present DCS in the ESEP model at 1.8, 2.1, and 3 eV. The experimental points are from Tanaka, Srivastava, and Chutjian (Ref. [9]) (×, circled crosses for extrapolated values) and Jung *et al.* (Ref. [15]) (Δ). The latter have been multiplied by a factor of 2.

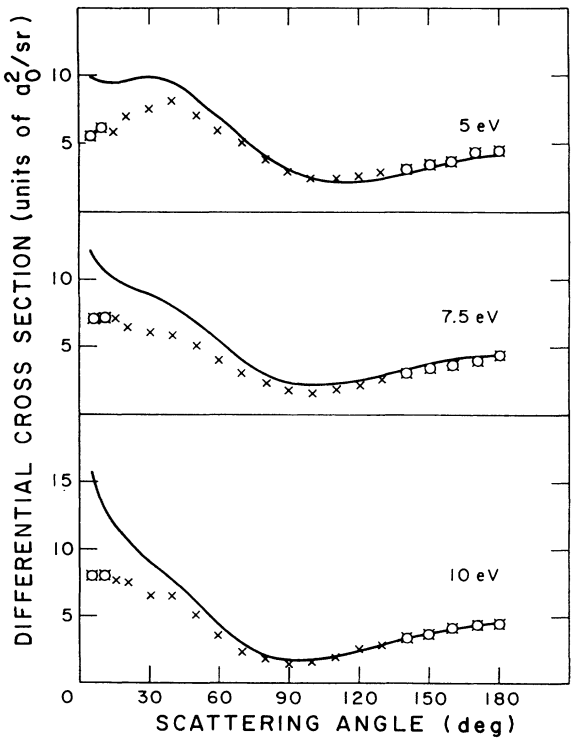

FIG. 8. As Fig. 7, but for 5, 7.5, and 10 eV.

of the elastic DCS at a relatively low energy (0.165 eV), and compared their values with the modified-effective-range theory (MERT) [69,70]. The shape of the observed DCS at 0.165 eV suggests that the $l_t=0$ (large-angle contributions) and $l_t=1$ (small-angle contribution) transitions largely determine this shape. The $l_t=2$ transitions contribute around intermediate angles (see Fig. 1 of Sohn *et al.* [16]). In Fig. 9, we show our ESEP results at 0.165 eV along with their observations. We confirm the results of their analysis, i.e., that *s*-wave scattering contributes significantly relative to the dipole term, while small-angle scattering is still dominated by the long-range dipole interaction. The calculated ESEP cross section in Fig. 9 is, for angles $\lesssim 20°$, within a few percent of the FBA cross section for the dipole transition. Again we note that our results seem to be in good agreement with measured results except in the forward direction.

Jung *et al.* [15] investigated individual differential cross sections for rotational excitation by unfolding rotationally broadened energy-loss spectra from crossed-beam measurements using a high-J approximation. There have also been quite a few theoretical attempts [22–32] to determine cross sections for rotational excitation of CO by electron impact. Chang [71] has developed an empirical approach to the determination of rotational-

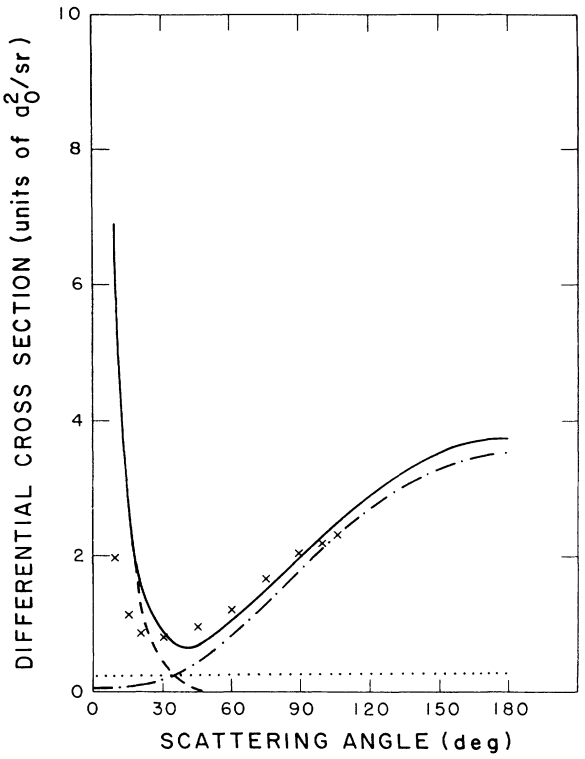

FIG. 9. DCS for *e*-CO scattering at 0.165 eV. The experimental points (×) are from Sohn *et al.* (Ref. [16]). At this energy the DCS is independent of the initial rotational state for angles greater than a few degrees. The present result is decomposed into contributions for $l_t=0$ (—·—·—·), $l_t=1$ (— — —), and $l_t=2$ (· · ·).

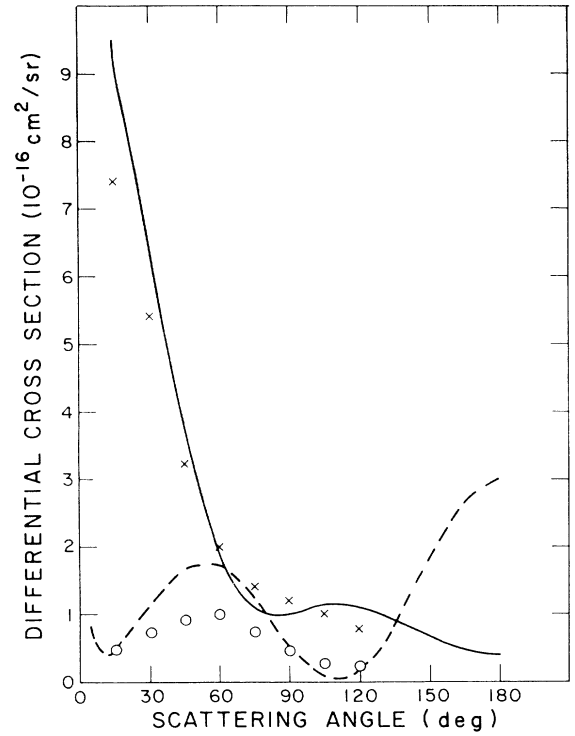

FIG. 10. Rotationally elastic ($l_t=0$, ——) and inelastic ($l_t=1$, — — —) differential cross sections at 1.8 eV in the present ESEP model. The experimental points are the results of the analysis by Jung *et al.* (Ref. [15]) for the $\Delta J=0$ (×) and $\Delta J=\pm 1$ (○) transitions. Note that the experimental numbers have been multiplied by a factor of 2.

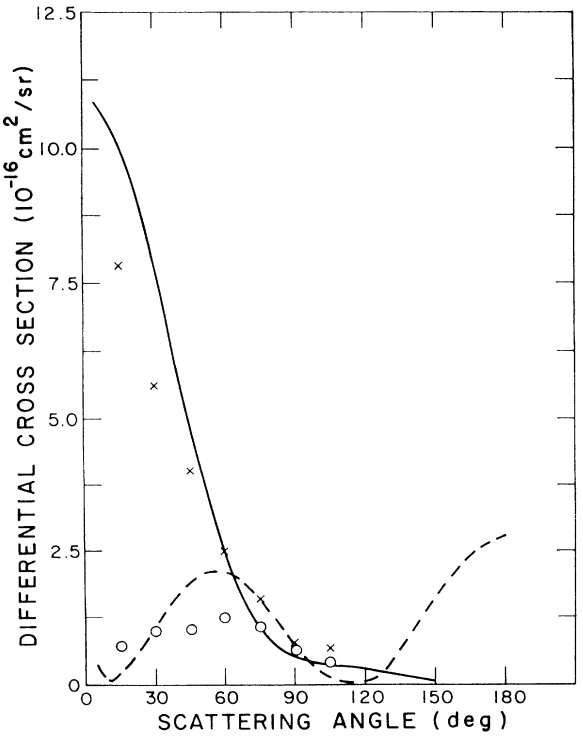

FIG. 11. As for Fig. 10, but at 2.1 eV.

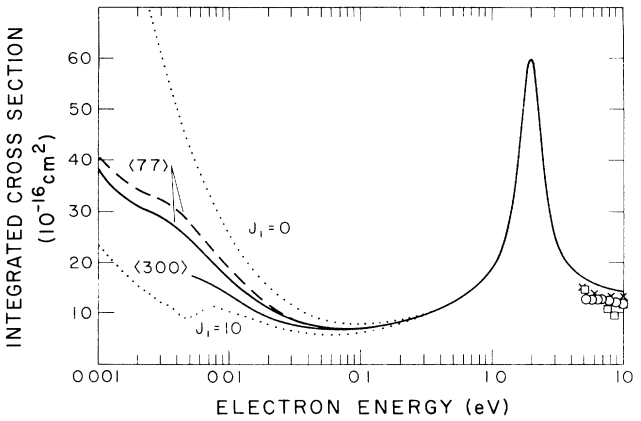

FIG. 12. Integrated cross sections for *e*-CO collisions: ——, present thermally averaged ESEP results; — — —, FBA results for energy below 0.1 eV; · · ·, results for a particular initial rotor state summed over all final states. Experiment: □, Tanaka, Srivastava, and Chutjian (Ref. [9]); ×, Kwan *et al.* (Ref. [12]); ○, Sueoka and Mori (Ref. [13]).

vibrational DCS for *e*-CO scattering at low energies. The measurements of Jung *et al.* [15] on the absolute total DCS near the resonance region at 1.8 and 2.1 eV in the angular range 15–120° are compared in Figs. 10 and 11, respectively, for the rotationally elastic ($l_t=0$) and inelastic ($l_t=1$) cases. Again the experimental points are renormalized by multiplying by a factor of 2.

2. *Integrated cross sections*

Our final σ_t values are shown in Figs. 12 and 13, and compared with recent measurements [10,12–14]. The semiempirical SMEP results of Chandra [30] do not agree with the overall shape of the experimental curve, while the present ESEP curve (solid line) agrees very well at all

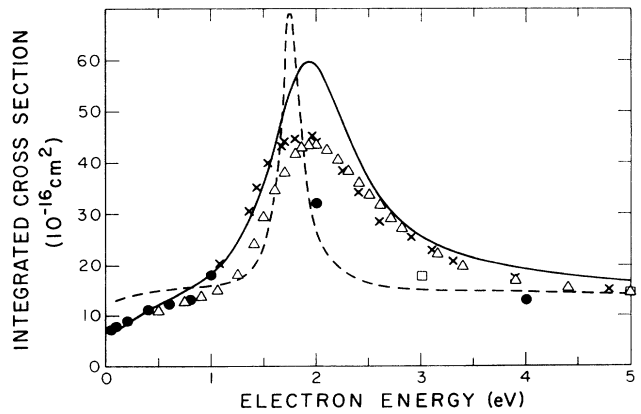

FIG. 13. As Fig. 12. The resonance region is shown for the present results (——) along with the calculations of Chandra (Ref. [30]) (— — —). Experiment: ●, Gus'kov, Savvov, and Slobodyanyuk (Ref. [11]); ×, Kwan *et al.* (Ref. [12]); Δ, Buckman and Lohman (Ref. [14]); □, Tanaka, Srivastava, and Chutjian (Ref. [9]).

energies. One can see (Table III) that the present E_r and Γ values for the $^2\Pi$ resonance are in very good agreement with measurements. However, a significant discrepancy (about 30%) around 2 eV with respect to magnitude of the cross section exists, for reasons not known with certainty. We note the much larger discrepancy between calculated and measured DCS (Fig. 7) in the vicinity of the resonance.

Some of this discrepancy may be due to the neglect of vibrational motion in the present model and also due to the approximation involved in the polarization potential. The CO molecule is known to have structure in vibrational excitation near the $^2\Pi$ resonance similar to that for electron scattering by N_2; however, the rich structure seen in σ_t for N_2 is not as apparent in the case of CO (see, for example, Ref. [18]). Apart from this oscillatory feature of σ_t in the N_2 resonance region, the discrepancy between the magnitude of the theoretical and experimental total cross section data in the resonance region of N_2 and CO is quite similar if the vibrational motion is neglected through the use of the FNA. Even a vibrational averaging procedure of the FNA amplitudes [72] will not resolve this discrepancy around 2 eV. Thus, we expect that a proper vibrational close-coupling calculation might be required in order to reduce significantly the present FNA σ_t for CO.

It is also possible that error is introduced in some measurements of σ_t due to a forward-angle discrimination problem. However, in a recent time-of-flight (TOF) electron-transmission experiment by Buckman and Lohmann [14], error due to an inadequate forward-scattering discrimination has been reduced to less than 0.1%. It is interesting to note that in the resonance region only two recent measurements, i.e., those of Kwan *et al.* [12] and Buckman and Lohmann [14], are close to each other; all other experimental data [10,11,13] are lower (about 30%) than the results of these two measurements. The integrated cross sections obtained [9] by extrapolating and integrating measured differential cross sections are in good agreement with those of Refs. [12] and [14] at only one point, 5.0 eV. It seems that the very old measurements of Refs. [3–5] suffered from poor angular resolution; the low values of Ref. [13] are probably due to insufficient energy resolution, while the data of Ref. [10] may be low due to uncertainties in their normalization procedure.

The results in the low-energy region (below 0.1 eV) are particularly interesting. The dependence on the initial rotor state becomes very important, and the thermally averaged cross section becomes correspondingly dependent on T. This might at first be interpreted to suggest that the modified form of the FNA used in the present work is unreliable. Note, however, that the total integrated cross section in this energy region is dominated by transitions for which $l_t=1$, i.e., dipole transitions. For these transitions the correction term in Eq. (4) is quite small, and the FBA is accordingly a good approximation. Since this is evaluated in the laboratory frame, the use of the FNA introduces only a small correction term. This is illustrated by the thermally averaged (at 77 K) FBA cross section shown in Fig. 12 for energies below 0.1 eV. (For energies above 0.1 eV the results of the present calculations and the FBA disagree to a greater extent as energy increases.)

3. *Momentum-transfer cross sections*

Our momentum-transfer cross sections σ_m are displayed in Fig. 14, and are compared with the swarm data [19,20]. Here the SMEP calculations of Chandra [30] are in somewhat better agreement with measured results and also with our calculations. The R-matrix calculations of Salvini, Burke, and Noble [36] (not shown) agree very well with our σ_m values in the resonance region. For example, at the $^2\Pi$ resonance position our σ_m value of 49.3 Å^2 is in good agreement with the R matrix value of 53.0 Å^2. On the other hand, below 1 eV the calculations of Salvini, Burke, and Noble [36] are much too large, perhaps due to the fact that in this low-energy region s-wave scattering is dominated by strong long-range polarization effects, neglected in their model. From the comparison of our very-low-energy results with the swarm data, it seems that the effect of neglecting the vibrational motion and the inaccuracy in the Hartree-Fock description of CO, other possibilities they hypothesized, may not be the reasons for this large discrepancy between the experiment and the R-matrix calculations of Salvini, Burke, and Noble [36].

The present ESEP curve in Fig. 14 compares well with the data of Hake and Phelps [17] and Land [19] except below 0.05 eV. At the energy of 0.025 eV, the present value of 2.99 (in units of 10^{-16} cm^{-2}) for $\langle \sigma_m \rangle_{77}$ can be compared with the measured values of 3.0 (Tice and Kivelson [73]) and 5.6 (Hake and Phelps [19]). In the resonance region (around 2 eV) the agreement between present theory and the swarm results is rather good with respect to both shape and magnitude. Above 4 eV our σ_m cross section is higher than the estimates of Land [19]. At such higher energies the analysis of the swarm

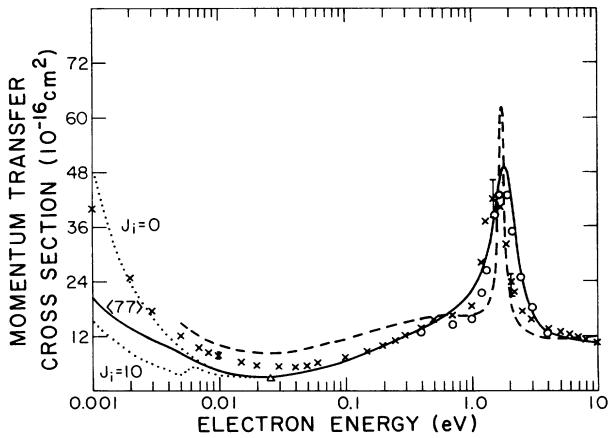

FIG. 14. Momentum-transfer cross sections for e-CO scattering. Theoretical data are the same as in Figs. 12 and 13. Experiment: ×, Land (Ref. [19]); ○, Haddad and Milloy (Ref. [20]); Δ, Tice and Kivelson (Ref. [73]).

experiments may not be accurate enough to yield the correct behavior of the cross sections, but there is other evidence (see Figs. 8 and 12) that the calculations may be a little too high above 5 eV.

Again the low-energy region, expanded in Fig. 15, is of considerable interest. There is a greater dependence on initial rotor states and temperature at low energies, but it is not nearly so pronounced as for the integrated cross section. Here again, the correction term arising from the present calculation is relatively small, and thus the FBA appears to be a reasonable approximation for energies below 0.03 eV. The most probable rotor state at 77 K is $J_i=3$, and we show the total momentum-transfer cross section for this state along with the thermal average. The kink in the former cross section arises from the opening of the $J_f=4$ channel as electron energy increases, an effect washed out in the thermal average over the Boltzmann distribution of initial states.

The difference between the results of the present calculations and the cross section derived from analysis of swarm data is substantial below 0.05 eV, as already noted. There is reason to question whether this is a real effect or perhaps an artifact of assumptions made in the swarm analysis. This analysis is motivated by an assumption that [19] "a good separation of elastic and inelastic effects" is obtained by using collision frequencies referred to as momentum transfer and energy exchange, respectively. As can be seen from Fig. 15, the momentum-transfer cross section at low energies is, in fact, dominated by inelastic transitions. Thus while the effective momentum-transfer cross section inferred from the swarm analysis may be a useful construct, it is not clear, when inelastic processes dominate, that it is the same quantity as that defined, for example, by Eq. (11).

4. *Rotational transitions*

In Fig. 16 we have plotted our total cross sections for the dipole ($0\rightarrow1$ and $1\rightarrow2$) and quadrupole ($0\rightarrow2$) allowed rotational transitions. Several other calculations in various approximations are also shown in this figure. There are significant differences between our ESEP results and the SMEP calculations of Saha *et al.* [32]. The calculations of Saha used a simple repulsive wall for the inner region, and were carried out in the laboratory frame, as were those of Crawford and Dalgarno [24] and Chandra [30]. In these latter two calculations the potential itself was adjusted to reproduce a particular feature of the observed cross sections. Chandra tuned his potential to the position of the $^2\Pi$ resonance, while Crawford and Dalgarno tuned theirs to reproduce the observed momentum-transfer cross section. While the present calculations used a much more accurate representation of the interaction potential, they were carried out in the molecular body frame with the FNA.

All three calculations shown in Fig. 16 are in quite reasonable agreement with regard to the dipole ($\Delta j=\pm1$) transitions, as might be expected, since these cross sections are dominated by small-angle scattering, for which the FBA is a good approximation. The good agreement between the present results and those of Crawford and Dalgarno may be due to the fact that their potential was tuned so as to reproduce the measured momentum-transfer cross section for energies between 0.005 and 0.1 eV, a region for which the $\Delta j=0$ and ±1 contributions dominate.

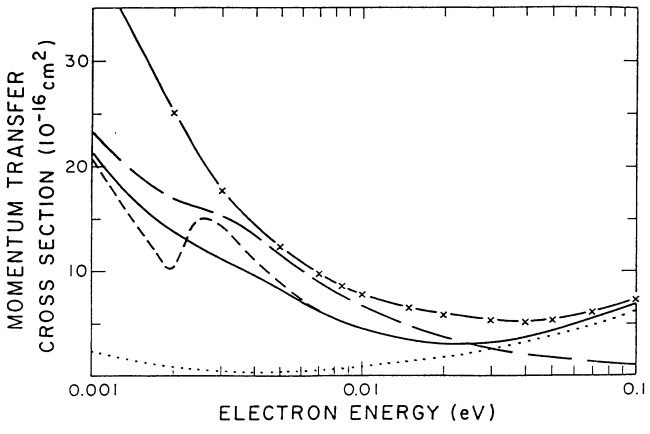

FIG. 15. Momentum-transfer cross section for *e*-CO scattering. Theoretical data: ——, present thermally averaged ESEP result for $T=77$ K; — —, FBA results also thermally averaged at 77 K; — — —, present ESEP result for $J_i=3$ summed over all final rotor states; · · ·, present ESEP result for $J_i=3$ to $J_f=3$; Experiment: —×—, Hake and Phelps (Ref. [17]).

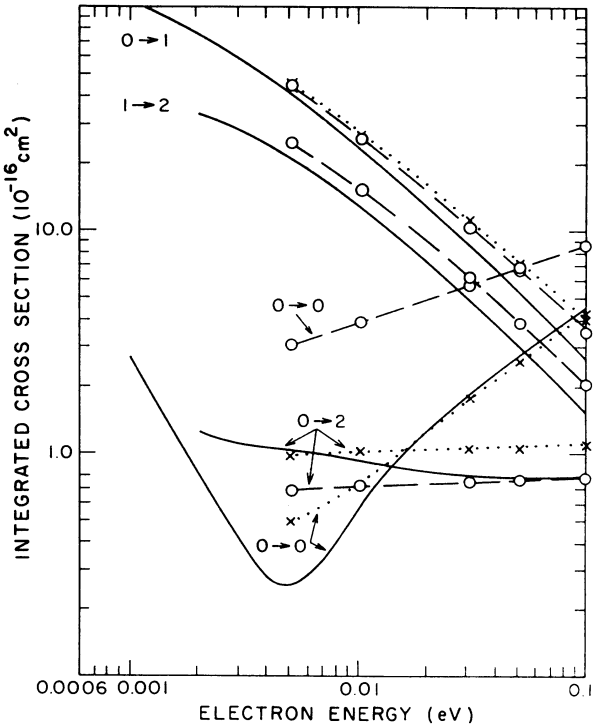

FIG. 16. Rotationally inelastic total cross sections for the $0\rightarrow0$, $0\rightarrow1$, $0\rightarrow2$, and $1\rightarrow2$ transitions in the ESEP model (——). Other theoretical data: · · · × · · ·, Crawford and Dalgarno (Ref. [24]); ○, Chandra (Ref. [30]).

IV. CONCLUDING REMARKS

In this paper we have reported rotationally elastic, inelastic, and averaged differential, integral, and momentum-transfer cross sections for electron collisions with CO in an energy range of 0.005–10 eV. A single-center integral-equation approach is adopted in which exchange is treated exactly and the polarization effects in a parameter-free way via the correlation-polarization model of O'Connell and Lane. The resulting cross sections for all the processes are compared with measured values.

Our results for the $^2\Pi$ shape resonance are excellent with respect to both position and width when compared with recent crossed-beam measurements. As for N_2, this resonance position is strongly affected by the short-range exchange interaction, but is shifted down by about 1.5 eV and reduced in width by about a factor of 2 when polarization effects are introduced. This provides strong support for the model [43] of the short-range correlation polarization interaction used in the present work.

Our results also confirm the importance of the long-range polarization interaction, particularly at low energies, but also suffer somewhat for forward scattering at low energies from the poor representation of the molecular dipole moment in the Hartree-Fock wave function.

Agreement with measured cross sections is generally reasonably good. However, we face some difficulties in the resonance region: our σ_t values of the peak are about 30% higher than the most recent measurements of Buckman and Lohmann [14], in which the possibility of any error due to forward-angle discrimination has been minimized, and about a factor of 2 larger than measurements [15] of DCS. It seems that the nuclear vibrational motion, which is neglected in the present study, plays an important role in the resonance region. A proper vibrational close-coupling calculation will be required in order to resolve this discrepancy.

Note added in proof. The paper by G. Ramanan and G. R. Freeman [J. Chem. Phys. **95**, 4195 (1991)] reports measurements of the momentum-transfer cross section in the energy range 0.002–0.3 eV that are in very good agreement with the present results (the solid curve in Figs. 14 and 15).

ACKNOWLEDGMENTS

This work was supported by the U.S. Department of Energy (Division of Chemical Sciences). We also acknowledge partial support by the Florida State University SCRI (Supercomputer Computation Research Institute) facility, which is partially funded by the U.S. Department of Energy through Contract No. DE-FC05-85ER250000. We thank N. T. Padial, M. Tronc, A. V. Phelps, S. Morgan, and S. Buckman for useful discussions and comments on our study. We also extend our thanks to the group of H. Ehrhardt for providing their experimental data in tabular form.

[1] J. W. Rich, in *Applied Atomic Collision Physics,* edited by E. W. McDaniel and W. L. Nighan (Academic, New York, 1982), Vol. 3, Chap. 4.
[2] D. W. Norcross, in *Applied Atomic Collision Physics,* edited by H. S. W. Massey, E. W. McDaniel, and B. Bederson (Academic, New York, 1981), Vol. 2, Chap. 13.
[3] E. Brüche, Ann. Phys. (Leipzig) **83**, 1065 (1927).
[4] C. Ramsauer and P. Kollath, Ann. Phys. (Leipzig) **12**, 529 (1932).
[5] F. L. Arnot, Proc. R. Soc. London Ser. A **133**, 615 (1931).
[6] H. Ehrhardt and K. Willmann, Z. Phys. **204**, 462 (1967).
[7] H. Ehrhardt, L. Langhans, F. Linder, and H. S. Taylor, Phys. Rev. **173**, 222 (1968).
[8] D. G. Truhlar, W. Williams, and S. Trajmar, J. Chem. Phys. **57**, 4307 (1972).
[9] H. Tanaka, S. K. Srivastava, and A. Chutjian, J. Chem. Phys. **69**, 5329 (1978).
[10] C. Szmytkowski and M. Zubek, Chem. Phys. Lett. **57**, 105 (1978); M. Zubek and C. Szmytkowski, Phys. Lett. **74** A, 60 (1979).
[11] Yu. K. Gus'kov, R. V. Savvov, and V. A. Slobodyanyuk, Fiz. Plazmy **4**, 941 (1977) [Sov. J. Plasma Phys. **4**, 527 (1978)].
[12] Ch. K. Kwan, Y. -F. Hsieh, W. E. Kauppila, S. J. Smith, T. S. Stein, and M. N. Uddin, Phys. Rev. A **27**, 1328 (1983).
[13] O. Sueoka and S. Mori, J. Phys. Soc. Jpn. **53**, 2491 (1984).
[14] S. J. Buckman and B. Lohmann, Phys. Rev. A **34**, 1561 (1986).
[15] K. Jung, Th. Antoni, R. Müller, K. -H. Kochem, and H. Ehrhardt, J. Phys. B **15**, 3535 (1982).
[16] W. Sohn, K. -H. Kochem, K. Jung, H. Ehrhardt, and E. S. Chang, J. Phys. B **18**, 2049 (1985).
[17] R. D. Hake and A. V. Phelps, Phys. Rev. **158**, 70 (1967).
[18] A. V. Phelps, Rev. Mod. Phys. **40**, 399 (1968).
[19] J. E. Land, J. Appl. Phys. **49**, 5716 (1978). Below 0.3 eV, Land quotes the results of Ref. [17].
[20] G. N. Haddad and H. B. Milloy, Aust. J. Phys. **36**, 473 (1984).
[21] K. D. Jordan and P. D. Burrow, Acct. Chem. Res. **11**, 341 (1978).
[22] Y. Singh, J. Phys. B **3**, 1222 (1970).
[23] Y. Itikawa and K. Takayanagi, J. Phys. Soc. Jpn. **26**, 1254 (1969).
[24] O. H. Crawford and A. Dalgarno, J. Phys. B **4**, 494 (1971).
[25] D. G. Truhlar and F. A. Van-Catledge, J. Chem. Phys. **59**, 3207 (1973).
[26] D. G. Truhlar and F. A. Van-Catledge, J. Chem. Phys. **69**, 3575 (1980).
[27] N. Chandra and F. A. Gianturco, Chem. Phys. Lett. **24**, 326 (1974).
[28] P. G. Burke, N. Chandra, and F. A. Gianturco, Mol. Phys. **27**, 1121 (1974).
[29] N. Chandra, Phys. Rev. A **12**, 2342 (1975).
[30] N. Chandra, Phys. Rev. A **16**, 80 (1977).
[31] K. Onda and D. G. Truhlar, J. Chem. Phys. **73**, 2688 (1980).
[32] S. Saha, S. Ray, B. Bhattacharya, and A. K. Barua, Phys. Rev. A **23**, 2926 (1981).
[33] D. A. Levin, A. W. Fliflet, and V. McKoy, Phys. Rev. A **21**, 1202 (1980).
[34] L. A. Collins, W. D. Robb, and M. A. Morrison, Phys.

Rev. A **21**, 488 (1980).
[35] N. Chandra, J. Phys. B **15**, 4465 (1981).
[36] S. Salvini, P. G. Burke, and C. J. Noble, J. Phys. B **17**, 2549 (1984).
[37] L. A. Collins and B. I. Schneider, in *Electron-Molecule Scattering and Photoionization,* edited by P. G. Burke and J. B. West (Plenum, New York, 1988), p. 147.
[38] S. J. Buckman, M. J. Brunger, D. S. Newman, G. Snitchler, S. Alston, D. W. Norcross, M. A. Morrison, B. C. Saha, G. Danby, and W. -K. Trail, Phys. Rev. Lett. **65**, 3253 (1990).
[39] See N. F. Lane, Rev. Mod. Phys. **52**, 29 (1980); L. A. Collins and D. W. Norcross, Adv. At. Mol. Phys. **18**, 341 (1982).
[40] L. A. Collins and D. W. Norcross, Phys. Rev. A **18**, 467 (1978).
[41] A. Jain and D. W. Norcross, in *Abstracts of Contributed Papers, Fourteenth International Conference on the Physics of Electronic and Atomic Collisions, Palo Alto, 1985,* edited by M. J. Coggiola, D. L. Huestis, and R. P. Saxon (North-Holland, Amsterdam, 1986), p. 214.
[42] B. I. Schneider and L. A. Collins. Phys. Rev. A **24**, 1264 (1981); T. N. Rescigno and A. E. Orel, *ibid.* **24**, 1267 (1981).
[43] J. O'Connell and N. F. Lane, Phys. Rev. A **27**, 1893 (1983); N. T. Padial and D. W. Norcross, *ibid.* **29**, 1742 (1984).
[44] N. T. Padial, D. W. Norcross, and L. A. Collins, J. Phys. B **14**, 2901 (1981).
[45] A. Jain and D. W. Norcross, Phys. Rev. A **32**, 134 (1985).
[46] A. Jain and D. W. Norcross, J. Chem. Phys. **84**, 739 (1986).
[47] M. A. Morrison, N. F. Lane, and L. A. Collins, Phys. Rev. A **15**, 2186 (1977); M. A. Morrison and L. A. Collins, *ibid.* **17**, 918 (1978).
[48] N. T. Padial and D. W. Norcross, Bull. Am. Phy. Soc. **30**, 147 (1984).
[49] F. W. Bobrowicz and W. A. Goddard, in *Methods of Electron Structure,* edited by H. F. Schaefer (Plenum, New York, 1977), Vol. 3, p. 77.
[50] L. A. Collins and B. I. Schneider (private communication).
[51] H. J. Werner and W. Meyer, J. Chem. Phys. **31**, 855 (1976).
[52] A. D. McLean and M. Yoshmine, Int. J. Quantum Chem. **1S**, 313 (1967).
[53] N. J. Bridge and A. D. Buckingham, Proc. R. Soc. London, Ser. A **295**, 334 (1966).
[54] J. E. Greedy, G. B. Bacskay, and N. S. Hush, Chem. Phys. **31**, 467 (1978).
[55] B. J. Ransil, Rev. Mod. Phys. **32**, 239 (1960).
[56] B. Rosenblum, A. H. Nethercrot, Jr., and C. H. Townes, Phys. Rev. **109**, 400 (1958); C. A. Burrus, J. Chem. Phys. **28**, 427 (1958).
[57] W. L. Meerts, F. H. De Leeuw, and A. Dymanus, Chem. Phys. **22**, 319 (1977).
[58] G. Herzberg, *Spectra of Diatomic Molecules* (Van Nostrand, New York, 1950).
[59] J. Kendrick, J. Phys. B **11**, L601 (1978).
[60] G. H. F. Diercksen, B. O. Roos, and A. D. Sadlej, Chem. Phys. **59**, 29 (1981); G. H. F. Diercksen and A. D. Sadlej, *ibid.* **96**, 17 (1985).
[61] K. K. Sunil and K. D. Jordan, Chem. Phys. Lett. **145**, 377 (1988).
[62] R. D. Amos, Chem. Phys. Lett. **68**, 536 (1979).
[63] D. W. Norcross and N. T. Padial, Phys. Rev. A **25**, 226 (1982); D. W. Norcross, *ibid.* **25**, 764 (1982).
[64] G. J. Schulz, Phys. Rev. A **135**, 988 (1964).
[65] M. Tronc, R. Azria, and Y. LeCoat, J. Phys. B **13**, 2327 (1980).
[66] G. J. Schulz, Rev. Mod. Phys. **45**, 378 (1973).
[67] J. R. Taylor, *Scattering Theory* (Krieger, Malabar, FL, 1972).
[68] A. K. Kazansky and I. S. Yelets, J. Phys. B **17**, 4767 (1984).
[69] T. F. O'Malley, Phys. Rev. **130**, 1020 (1962).
[70] E. S. Chang, J. Phys. B **14**, 893 (1981); E. S. Chang, Th. Antoni, K. Jung, and H. Ehrhardt, Phys. Rev. A **30**, 2086 (1984).
[71] E. S. Chang, Phys. Rev. A **16**, 1850 (1977).
[72] B. C. Saha, in *Electron-Molecule Scattering and Photoionization* (Ref. [37]), p. 221.
[73] R. Tice and D. Kivelson, J. Chem. Phys. **46**, 4748 (1967).